



# Thermal decomposition of inclusion compounds and metal–organic frameworks on the basis of heterometallic complex $[\text{Li}_2\text{Zn}_2(\text{bpdc})_3]$

Vladimir Logvinenko<sup>1,2</sup> · Aleksandr Sapiyanik<sup>1,2</sup> · Denis Pishchur<sup>1</sup> · Vladimir Fedin<sup>1,2</sup>

Received: 12 October 2018 / Accepted: 5 March 2019 / Published online: 19 March 2019  
© Akadémiai Kiadó, Budapest, Hungary 2019

## Abstract

Metal–organic frameworks (MOFs) have promising practical applications in gas storage, separation and purification and catalysis. The standard process for MOF production begins with the synthesis of the inclusion compound. The molecules of the organic solvent used are caught in the channels and caves of the MOF structure. These primary inclusion guest molecules are excluded further by the weak heating or by the evacuation. The thermal stability of the primary inclusion compounds (i.e., the ease of removal of the guest molecules) must be connected both with the structure of the empty (guest free) frameworks and with the size of the guest molecules. We investigate a series of inclusion compounds:  $[\text{Li}_2\text{Zn}_2(\text{bpdc})_3(\text{dabco})] \cdot 9\text{DMF} \cdot 4\text{H}_2\text{O}$ ,  $[\{\text{LiZn}\}_2(\text{bpdc})_3(\text{dma})_4] \cdot 3\text{DMA} \cdot \text{H}_2\text{O}$  and  $[\{\text{LiZn}\}_2(\text{bpdc})_3(\text{nmp})_4] \cdot 4\text{NMP}$  ( $\text{bpdc}^{2-} = \text{C}_{14}\text{H}_8\text{O}_4^{2-}$  anion,  $\text{dma} = \text{C}_4\text{H}_9\text{NO}$ ,  $\text{nmp} = \text{C}_5\text{H}_9\text{NO}$ ,  $\text{dmf} = \text{C}_3\text{H}_7\text{NO}$  and  $\text{dabco} = \text{C}_6\text{H}_{12}\text{N}_2$ ) for the study of the correlation between their kinetic stability and the framework and guest molecule properties. Thermodynamic properties were studied using differential scanning calorimeter Netzsch DSC 204 F1 Phoenix. Thermogravimetric measurements were carried out on a Netzsch thermal analyzer TG 209 F1. Thermogravimetric curves are used for the kinetic studies. Kinetic parameters of decomposition are estimated within the approaches of non-isothermal kinetics (“model-free” kinetics and nonlinear regression methods), with the computer program Netzsch Thermokinetics 2. All guest-free frameworks turned out to be the unstable phases; the peculiarities of the thermal decomposition of the inclusion compounds under these circumstances are considered.

**Keywords** Inclusion compounds · Kinetic stability · Metal–organic frameworks · Non-isothermal kinetics

## Introduction

The coordination chemistry is well-known up-to-date field of fundamental scientific knowledge. With respect to the solution chemistry,—thousands reactions were investigated: both complex formation, and substitution reactions in coordination spheres. Respective equilibrium constants

(both enthalpy, and entropy contributions) were calculated. Respective rate constants (both activation energies and pre-exponent factors) were calculated too.

With respect to the solid state chemistry,—thousands coordination compounds, cluster compounds and inclusion compounds were synthesized, their single crystals were grown, and thousands structures were solved. Real reliable constructions of coordination spheres (with ligands location) and metal–organic frames were getting just from the solid state.

Many new coordination compounds and inclusion compounds are continuously synthesized; the crystal structure identification is the mandatory requirement. The thermal decomposition processes are usually studied, but the thermodynamic and (or) the kinetic stability investigation is rather rare [1–16].

Metal–organic coordination polymers are compounds with infinite structures built from organic and inorganic units. Porous metal–organic frameworks (MOF) are now of

**Electronic supplementary material** The online version of this article (<https://doi.org/10.1007/s10973-019-08173-0>) contains supplementary material, which is available to authorized users.

✉ Vladimir Logvinenko  
val@niic.nsc.ru

<sup>1</sup> Nikolaev Institute of Inorganic Chemistry, Siberian Branch of Russian Academy of Sciences, Ac. Lavrentyev Ave 3, Novosibirsk-90, Russia 630090

<sup>2</sup> Novosibirsk State University, Pirogova St 2, Novosibirsk-90, Russia 630090

significant interest because of the wide opportunities of combining metals and ligands in their synthesis that allow for the production of coordination polymers with extended surface areas and the tuning of the size and shape of the pores [17, 18]. Depending on the structure, such materials can serve as matrices for the inclusion of specific guest molecules, which highlights their unique properties and various potential applications. Porous coordination polymers are widely studied as materials for gas storage, separation, catalysts and sensors [19–28]. The ability of metal–organic frameworks to include ions and molecules of different sizes leads to their application in ion exchange, drug delivery, proton conductivity [29–32] and other areas. All these potential applications are determined not only by the attributes of the framework itself, but also by the interaction of the coordination polymer and guest molecules. The presence of the guest molecules can have a significant influence on the coordination polymer structure [33] and greatly contribute to the properties of the resulting inclusion compound [34]. Thus, for the investigation of the properties of a host–guest system, the metal–organic framework and the guest composition should be studied in complex. Versatile research on this topic is important for the understanding the principles of host–guest interactions, discovering new properties and extending the scope of hybrid porous materials.

The interaction between the guest molecules and the framework in such supramolecular compounds is generally due to van der Waals forces. The thermal stability of the primary inclusion compounds (i.e., the ease of removal of the guest molecules) can be connected both with the structure of the empty (guest free) frameworks and with the size of the guest molecules. Therefore, we studied the correlation between the kinetic stability (usually called thermal stability) of the inclusion compounds and the properties of both the frameworks and guest molecules.

The standard process for metal–organic frames production begins from the synthesis of the inclusion compound. The molecules of the organic solvent used are caught in the channels and cavities of the as-synthesized coordination polymer structure. These primary entrapped guest molecules are excluded further by the evacuation or by weak heating in a process known as framework activation. It appears that certain obtained guest-free frameworks of the inclusion compounds (empty structures) are thermodynamically and kinetically unstable, do not exist and decomposed into the simple coordination compounds.

The series of such inclusion compounds were studied earlier [33–37] and are studied in this paper.

## Experimental

### Thermal analysis

The study of the kinetic stability of compounds includes the obtaining of the thermal kinetic curves and their mathematical treatment.

Thermogravimetric measurements were carried out on a Netzsch thermal analyzer, TG 209 F1. The sample mass was  $m = 5.0 \pm 0.1$  mg; the open standard corundum sample holder was used. The experiments were performed under a helium flow ( $60 \text{ cm}^3 \text{ min}^{-1}$ ) at heating rates of 5, 10 and  $20 \text{ K min}^{-1}$ .

Such small sample mass reduces the self-cooling for the endothermic reactions; the self-cooling decreased the heating linearity. The selection of heating rates 5, 10 and  $20 \text{ K min}^{-1}$  is important: The lesser rates will not guarantee the satisfactory shift from the equilibrium, the greater rates will notably impair the heat transfer properties within the sample holder. The sample holder must be open, without a lid; the gas flow rates must be high (for the satisfactory shift from the equilibrium for the reversible reactions).

Thermodynamic properties were studied using differential scanning calorimeter NETZSCH DSC 204 F1 Phoenix. DSC measurements of the samples were performed by heat flow measurement method; heating/cooling rate was  $9 \text{ K min}^{-1}$ , argon flow  $25 \text{ sm}^3 \text{ min}^{-1}$  and standard aluminum crucible. Netzsch Proteus Analysis software was used to determine DSC peak area for further averaging the results of two experiments. Molar enthalpy of the decomposition,  $\Delta H$ , was calculated as the area of the DSC peak.

### Kinetic analysis under non-isothermal conditions

Thermogravimetric data were processed with Netzsch Thermokinetics 2 (Version 2004.05) [38, 39].

The mass loss stages are calculated from initial mass assuming certain stoichiometry, in concordance with the moles of removed water, DMF, dabco etc.; these percentage mass losses were recalculated to the conversion degrees ( $\alpha$ ), required for the kinetic parameters calculations. The temperature intervals correspond to these mass losses (from the ASCII-files).

A special program module, “model-free” (Friedman analysis), based on well-known studies [40–49], allows one to process multiple thermogravimetric curves obtained with different heating rates and calculate the apparent activation energy without preliminary information about the kinetic topochemical equation. The Friedman method was used to calculate the activation energies for each

experimental point of fractional conversion in the range  $0.005 < \alpha < 0.995$ . This method was created for the one-stage processes study, so if the activation energy is variable in compliance with the Friedman method, the decomposition process is a multistage reaction.

We used the same set of experimental data to search for the corresponding topochemical equation. The selection was made from 16 equations, involving chemical reactions at the interface, nucleation and diffusion.

The considered topochemical equations are different. The order equations  $f(x) = (1 - \alpha)^n$  ( $n = 0, 0.5, 0.67$ ) conform to the chemical reactions on the interface; Avrami–Erofeev equations  $f(x) = (1 - \alpha) \cdot [-\ln(1 - \alpha)]^n$  conform to the nucleation centers occurrence and growth; several diffusion equations (Jander equation, Ginstling–Brounstein equation, D2 and D3) conform the two-dimensional and three-dimensional gas diffusion processes. The Prout–Tompkins equations  $f(x) = (1 - \alpha) \cdot \alpha^n$  conform the processes with the autocatalysis.

These calculations were made by the improved differential procedure of Borchardt–Daniels [38, 39, 50], within the multiple linear regression approach.

The Fisher test [38] was used to search for the best kinetic description and for statistical control of the obtained equation. It tests the residual variance of individual models against one another and answers the question of whether the models differ significantly (statistically) or not. If  $F_{\text{exp}(1)} \approx F_{\text{exp}(2)}$  for two equations, there is no reason to assume the first model is better at characterizing the experiment. The statistical quantile,  $F_{\text{crit}}$ , is obtained for a level of significance of 0.05.

If the calculation results in two or three kinetic equations with close values in their correlation coefficients and in the  $F$  test, but with noticeably different values in kinetics parameters, it is best to choose the equation with activation energy values closest to the data from the “model-free” module program. Such discrimination is very relative in the search for topochemical equations, but it helps to find the most reliable ones. The special program of nonlinear regression [38, 39] is useful in searching for a full set of kinetic parameters for multistage processes. The closest fit between the activation energies from the “model-free” analysis and the nonlinear regression calculation is important from a physicochemical point of view.

Netsch Thermokinetics 2 enables estimation of the contribution of each stage (as the  $\Delta m$  portion) after the nonlinear regression calculation. This was useful for defining the composition for the intermediate phases in the multistage decomposition reactions.

Well-known recommendations for performing kinetic computations on thermal analysis data [51–60] were used.

There are several important assumptions and limitations. Any kinetic study is really the solution of the inverse

problem, so it is usually ill conditioned. The existence, uniqueness and stability of the solution are usually in doubt. The kinetic equations to calculate the kinetic parameters are topochemical ones, and the calculated parameters ( $E$  and  $A$ ) are formal and conventional from the standpoint of the classical chemistry of solids.

However, the general trend in the variation of these values within a selected series of compounds (either isostructural or genetically related) is very important because the expected disorder in the reaction zones can be identical. All errors will be minimized and smoothed in such a comparison. The appropriate series consists of coordination compounds with volatile ligands (with one central atom and different ligands or with different central atoms and the same ligand) [61, 62].

This approach was useful in the study of lignin-containing powder fuels, nanostructures of ultrafine and amorphous oxide materials, combustion processes for expanded graphites, dimensional effects on the composition and properties of polydicarbonfluorides, structural rearrangements of fluorinated graphite intercalates, the spin transition in iron complexes and the volatility of heterometallic  $\beta$ -diketonates [63–69].

The studied metal–polymer frameworks are formed by the  $[\text{Li}_2\text{Zn}_2(\text{bpdc})_3]$  coordination spheres, gathered into the crystal structures by the different linkers (dabco, dma and nmp); the included guests are a series of organic amines (DMF, DMA and NMP) and water molecules.

## Compound preparation and composition

The syntheses of the studied compounds and their structure were thoroughly described earlier [36]. The structures of all compounds were solved by a direct method and refined by the full-matrix least squares technique in the anisotropic approximation (except hydrogen atoms) using the SHELX-2014 software.

The final formulas of all compounds were derived from the SQUEEZE results, which were in a good agreement with C, H and N analysis (on Eurovector 600 analyzer). The activation of the compounds by heating in vacuum results in an amorphization of the crystalline material [36].

Studied compounds:  $[\text{Li}_2\text{Zn}_2(\text{bpdc})_3(\text{dabco})] \cdot 9\text{DMF} \cdot 4\text{H}_2\text{O}$ ,  $[\{\text{LiZn}\}_2(\text{bpdc})_3(\text{dma})_4] \cdot 3\text{DMA} \cdot \text{H}_2\text{O}$  and  $[\{\text{LiZn}\}_2(\text{bpdc})_3(\text{nmp})_4] \cdot 4\text{NMP}$  ( $\text{bpdc}^{2-} = \text{C}_{14}\text{H}_8\text{O}_4 = \text{biphenyl-4,4'-dicarboxylic anion}$ ,  $\text{DMF} = \text{C}_3\text{H}_7\text{NO} = \text{dimethyl formamide}$ ,  $\text{DMA} = \text{C}_4\text{H}_9\text{NO} = \text{dimethyl acetamide}$ ,  $\text{NMP} = \text{C}_5\text{H}_9\text{NO} = \text{N-methylpyrrolidone}$ ,  $\text{dabco} = \text{C}_6\text{H}_{12}\text{N}_2 = 1,4\text{-diazabicyclo}[2.2.2]\text{octane}$ ). The compounds  $[\{\text{LiZn}\}_2(\text{bpdc})_3(\text{dma})_4] \cdot 3\text{DMA} \cdot \text{H}_2\text{O}$  and  $[\{\text{LiZn}\}_2(\text{bpdc})_3(\text{nmp})_4] \cdot 4\text{NMP}$  are isostructural.

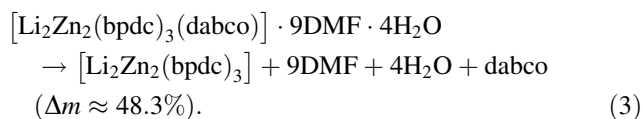
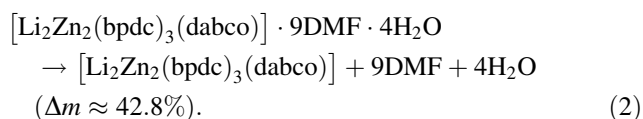
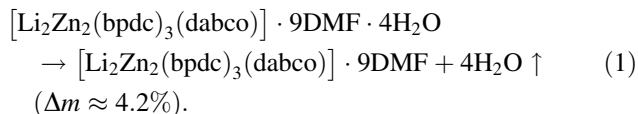
## Results and discussion

### Kinetic study

#### $[\text{Li}_2\text{Zn}_2(\text{bpdc})_3(\text{dabco})] \cdot 9\text{DMF} \cdot 4\text{H}_2\text{O}$

The metal–organic framework structure is highly porous with large cages of ca. 9Å, interconnecting by a windows of ca. 6 X 7Å (accessible volume—65%) [36].

The calculated mass losses for this formula under heating up to 473 K (Figs. 1, 2) are:



The simultaneously inclusion of dimethyl formamide and water molecules in the framework channels is usual for the inclusion compounds on the basis of metal–organic frameworks, based on the camphorate coordination compounds.  $[\text{Zn}_2(\text{camph})_2\text{dabco}] \cdot \text{DMF} \cdot \text{H}_2\text{O}$ ,  $[\text{Zn}_2(\text{camph})_2\text{bpy}] \cdot 3\text{DMF} \cdot \text{H}_2\text{O}$ ,  $[\text{Zn}_2(\text{camph})_2\text{bpe}] \cdot 5\text{DMF} \cdot \text{H}_2\text{O}$  ( $\text{H}_2\text{camph} = \text{C}_8\text{H}_{14}(\text{COOH})_2$ , dabco =  $\text{C}_6\text{H}_{12}\text{N}_2$ , bpy =  $\text{C}_{10}\text{H}_8\text{N}_2$ , bpe =  $\text{C}_{12}\text{H}_{10}\text{N}_2$ ) [52]. All these compounds lose these water molecules at the beginning of the heating [37].

We think that the studied inclusion compound loses the water molecules at the very beginning of the heating too and dimethyl formamide molecules later on. The forms of the TG-curve and DTG-curve correspond to this

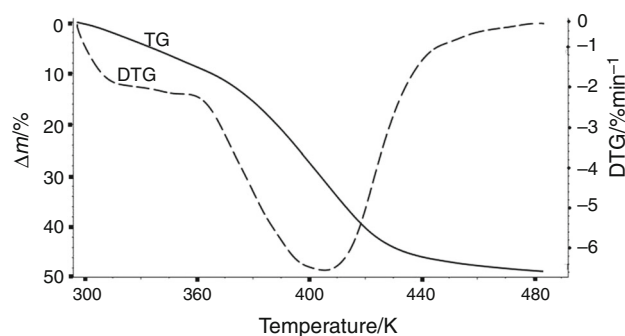


**Fig. 1** Thermal decomposition of  $[\text{Li}_2\text{Zn}_2(\text{bpdc})_2(\text{dabco})] \cdot 9\text{DMF} \cdot 3\text{H}_2\text{O}$ ; standard corundum sample holder; helium flow  $60 \text{ cm}^3 \text{ min}^{-1}$ ; heating rate  $10 \text{ K min}^{-1}$

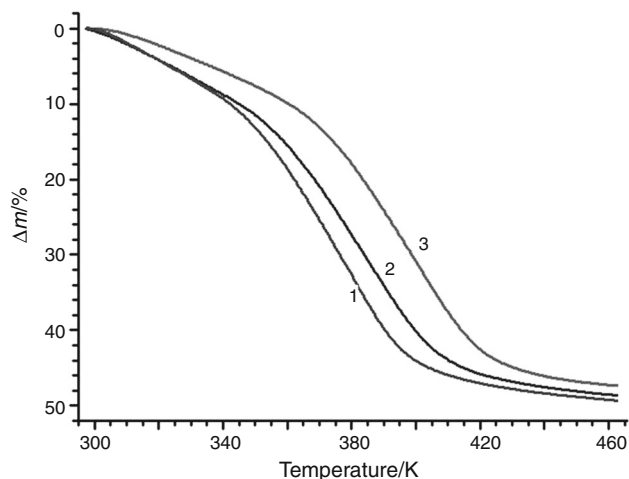


**Fig. 2** Thermal decomposition of  $[\text{Li}_2\text{Zn}_2(\text{bpdc})_2(\text{dabco})] \cdot 9\text{DMF} \cdot 3\text{H}_2\text{O}$ : mass loss curves; used for the kinetic analysis; standard corundum sample holder; helium flow  $60 \text{ cm}^3 \text{ min}^{-1}$ ; the heating rates were 5(1), 10(2) and 20(3)  $\text{K min}^{-1}$

consideration (Fig. 1). The mass loss of these four water molecules corresponds to  $\approx 4.2\%$ .

The “Model-free” data are shown in Fig. 3. The activation energy can be considered as variable in compliance with the Friedman method, so the decomposition process is the multistage reaction.

This set of three consecutive decomposition reactions is not possible to combine in the three-stage step for the joint kinetic analysis because of the different molar masses for water, dimethyl formamide and dabco. Therefore, we used the simple assumption for the kinetic analysis of the complicated decomposition process. The water removal is the first decomposition step (in the limits  $0.005 < \alpha < 0.087$  on the Friedman dependence), the next step is the removal of nine dimethyl formamide molecules (in the limits  $0.087 < \alpha < 0.886$  on the Friedman dependence), and the third step is the dabco molecules removal ( $0.886 < \alpha < 0.995$  on the Friedman dependence).

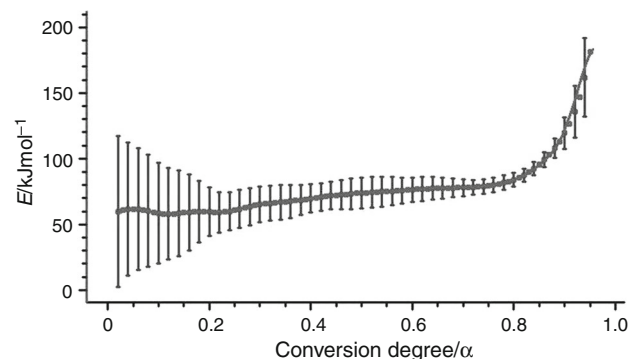
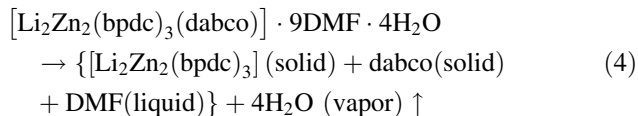
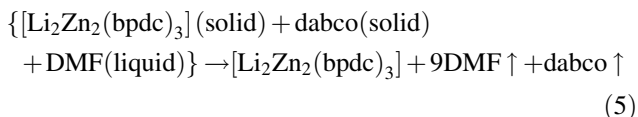


**Fig. 3** Friedman analysis of  $[\text{Li}_2\text{Zn}_2(\text{bpdc})_2(\text{dabco})] \cdot 9\text{DMF} \cdot 3\text{H}_2\text{O}$  thermal decomposition: activation energies depending on the degree of conversion  $\alpha$ . Perpendicular lines SD of calculation

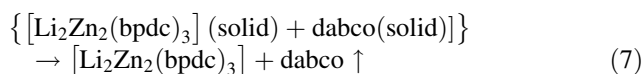
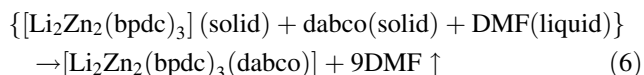
It is known that the guest-free framework is unstable, and the heating in vacuum results in an amorphization of the crystalline material [36]. The melting temperatures for DMF is 213 K, the melting temperature for dabco is 430 K, so we think that the real decomposition process begins (300–320 K) with the full breakup of the framework structure into the complex mixture:



We studied the kinetics of this dehydration process, but the mass loss is small, the errors are too big; we estimated the kinetic data (Fig S1), and will not discuss the details.

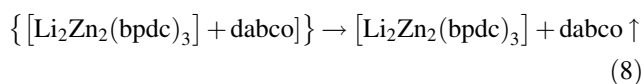


We try to consider the mass loss from 4.2% up to 48.3% (9 DMF + dabco) as the single step (Eq. 5), but the kinetic description was not satisfactory (Fig. S2). We used the calculated dependence on the time, not on the temperature, so as these curves are more obvious case. The boiling temperature and the vaporization temperature of dabco ligand are 430 K and 470 K, respectively. So we analyze the decomposition as two consecutive reactions (Eqs. 6–7):



The activation energy value can be considered constant in the limits  $0.087 < \alpha < 0.886$  (Fig. 3), in compliance with the mass loss from 4.2% up to 42.8% (Fig. 1); it means the single-stage process of the DMF removal (Eq. 6). The certain increase in the value in the end of the process is connected with the poorly divided reactions of DMF and dabco removal. The best description is Avrami–Erofeev equation An (Fig. 4, Fig. S3 and Table S1):

$$\begin{aligned} & \text{An}, f(\alpha) = (1-\alpha)/[-\ln(1-a)]^{0.9}, \\ & E = 74 \pm 2 \text{ kJ mol}^{-1}, \quad \lg A = 8.3 \pm 0.3. \\ & \text{Corr. coeff.} = 0.995019. \end{aligned}$$



The calculation was made for the degree of conversion  $0.886 < \alpha < 0.995$  (in compliance with the mass loss from 42.8% up to 48.3%). The best description is the single-stage process, Avrami–Erofeev equation An (Fig. 5 and Fig. S4):

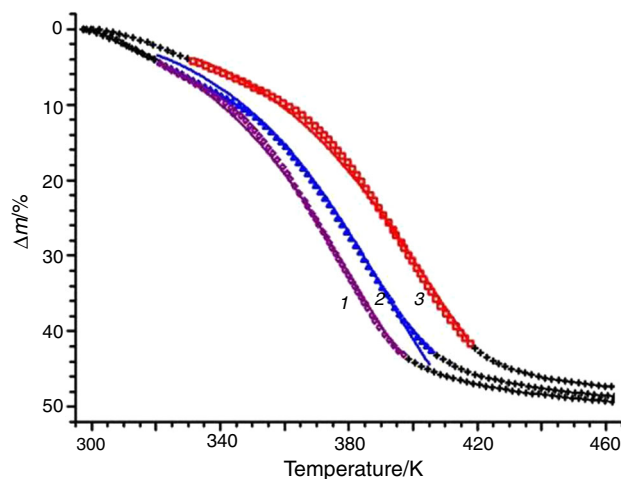


**Fig. 4** Data processing for  $[\text{Li}_2\text{Zn}_2(\text{bpdc})_2(\text{dabco})] \cdot 9\text{DMF} \cdot 3\text{H}_2\text{O}$  thermal decomposition (Eq. 6). TG curves fitting of nonlinear regression, simulated with the single-stage reaction. The points are the experimental data; the lines are the calculated data. The heating rates were 5 (1), 10 (2) and 20 (3)  $\text{K min}^{-1}$

$$\begin{aligned} & \text{An}, f(\alpha) = (1-\alpha)/[1 - (1-a)]^2, \quad E = 79 \pm 5 \text{ kJ mol}^{-1}, \\ & \lg A = 9.2 \pm 0.7. \end{aligned}$$

$$\text{Corr. coeff.} = 0.957112.$$

The decomposition of other inclusion compounds was not studied in details.

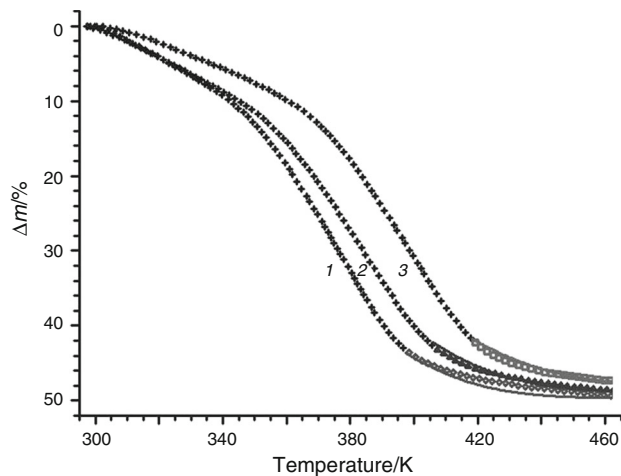
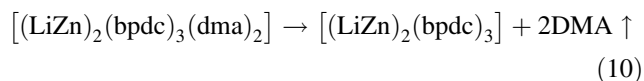
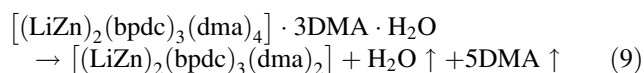


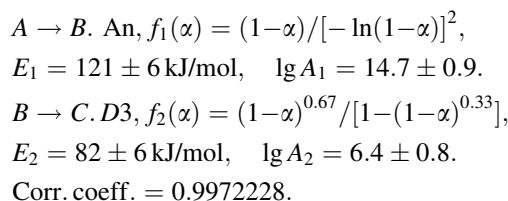
**Fig. 5** Data processing for  $[\text{Li}_2\text{Zn}_2(\text{bpdc})_2(\text{dabco})] \cdot 9\text{DMF} \cdot 3\text{H}_2\text{O}$  thermal decomposition (Eq. 8). TG curves fitting of nonlinear regression, simulated with the single-stage reaction. The points are the experimental data; the lines are the calculated data. The heating rates were 5 (1), 10 (2) and 20 (3)  $\text{K min}^{-1}$

### $[(\text{LiZn})_2(\text{bpdc})_3(\text{dma})_4] \cdot 3\text{DMA} \cdot \text{H}_2\text{O}$

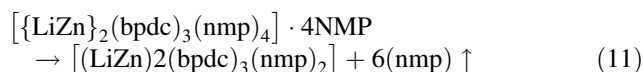


The calculated mass losses for this reaction under heating up to 473 K (Fig. S5) are 30.4% (Eq. 9) and 42.6% (Eq. 10), respectively. We studied the kinetics of the first decomposition reaction only.

The “Model-free” data are given in Fig. S6). The activation energy value can be considered constant in the limits  $0.00 < \alpha < 0.66$ , in compliance with the mass loss from 00.0% up to 30.4% (Fig. S5); it means the single-stage process of one water molecule and five DMA molecules simultaneous removal. The certain increase in the value in the end of the process is connected with the poorly divided reactions of the first and the next decomposition steps. The best description is the two-stage process with the consecutive reactions (Avrami–Erofeev equation and the equation of three-dimensional diffusion D3 (Fig. S7):



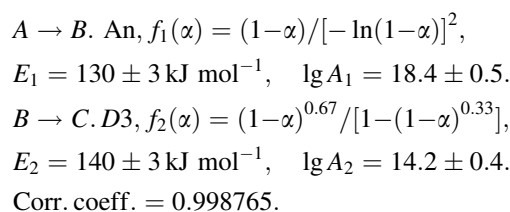
### $[(\text{LiZn})_2(\text{bpdc})_3(\text{nmp})_4] \cdot 4\text{NMP}$



The calculated mass loss for this reaction under heating up to 500 K (Fig. S8) is  $\Delta m \approx 36\%$ .

The “Model-free” data are given in Fig. S9. The activation energy can be considered as variable in compliance with the Friedman method, so the decomposition process is the multistage reaction. The decomposition with mass loss  $\approx 36\%$  corresponds to interval  $0.00 < \alpha < 0.75$ .

The best description is the two-stage process with the consecutive reactions (Avrami–Erofeev equation and the equation of three-dimensional diffusion D3 (Fig. S10):



### Thermodynamic study

We studied the heat effects only for  $[\text{Li}_2\text{Zn}_2(\text{bpdc})_3(\text{dabco})] \cdot 9\text{DMF} \cdot 4\text{H}_2\text{O}$  decomposition. The DSC peak is shifted to the higher temperature with respect to the DTG peak (Figs. 1, 6). It is connected with the difference in the experimental conditions. DSC experiment runs in the conditions more close to the equilibrium state (the sample was pressed in the aluminum crucible, the lid has perforations; the inert gas flow was low).

The total endothermic peak (300–460 K) corresponds to the water, DMF and dabco removal and the heat of phase transition (Fig. 6). This heat value ( $742 \text{ kJ mol}^{-1}$ ) fits to the vaporization heats of four water moles, nine DMF moles and one dabco mole ( $\approx 605 \text{ kJ mol}^{-1}$ ). But the values of the activation energies for these three decomposition processes are rather low:  $E_{\text{water}} = 103 \text{ kJ/mol}$ ,  $E_{\text{DMF}} = 70 \text{ kJ mol}^{-1}$  and  $E_{\text{dabco}} = 79 \text{ kJ mol}^{-1}$ .

We explain this by the full framework destruction during the water removal.  $E_{\text{water}} = 103 \text{ kJ/mol}$ , this value fits more or less with 4 water molecules removal, complicated and modified with the phase transition heat. But the explanation of DMF and dabco removal kinetics must be quite different. The dehydrated compound turns into the amorphous mass: the mixture of  $\text{Li}_2[\text{Zn}_2(\text{bpdc})_3]$  (solid) + dabco (solid) + DMF (liquid). The process of the DMF evaporation from this mixture is not the DMF removal from the framework structure, but the process of

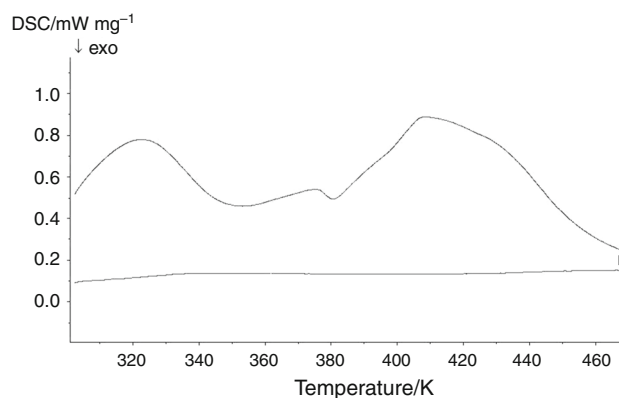


**Fig. 6** DSC curve for the full thermal decomposition of  $[\text{Li}_2\text{Zn}_2(\text{bpdc})_3(\text{dabco})] \cdot 9\text{DMF} \cdot 3\text{H}_2\text{O}$ ; open aluminum sample holder; argon flow  $40 \text{ cm}^3 \text{ min}^{-1}$ ; heating rate was  $9 \text{ K min}^{-1}$

the evaporation of DMF drop disposed in the Li[Zn(bpdc)] powder. Therefore, this value ( $\text{kJ mol}^{-1}$ ) will refer to the pure DMF mole.  $E_{\text{DMF}} = 70 \text{ kJ mol}^{-1}$  fits to the DMF evaporation heat ( $\Delta H_{\text{vapor}} = 42.3 \text{ kJ mol}^{-1}$ ). For dabco:  $T_{\text{melt}} = 430 \text{ K}$ ,  $T_{\text{vapor}} = 470 \text{ K}$ ; so the activation energy of dabco removal fits to the evaporation heat ( $61.9 \text{ kJ mol}^{-1}$ ).

It is important to add that these quantitative data on the vaporization kinetics are not the real description of liquids evaporation. The process depends considerably on the experimental conditions (gas pressure, thermal physic properties of the crucible and of the furnace, etc.). But any kinetic description will include the activation energy, dependent on the vaporization heat.

## Conclusions

The non-isothermal kinetics approach is formal and conventional from the standpoint of the classical chemistry of solids; the calculated kinetic parameters ( $E$  and  $A$ ) are formal and conventional too, but the comparison of such quantitative kinetic data is important for the comparison of the analogous decomposition reactions. If they are used for the description of the chemical process, the apparent activation energy for the endothermic thermal decomposition ( $A_{\text{solid}} \rightarrow B_{\text{solid}} + C_{\text{gas}} \uparrow$ ) will consist of the activation barrier, heat of the guest molecules evaporation ( $C_{\text{gas}} \uparrow$ ) and the phase transformation ( $A_{\text{solid}} \rightarrow B_{\text{solid}}$ ) heat. The contribution of the activation barrier and the phase transformation are uncertain, but must not be very big for the compounds on the basis of flexible structure of microporous metal–organic frameworks.

Therefore, we can expect that the apparent activation energy value must not be equal to the evaporation heat, but must correspond (more or less) to the evaporation heat of the included moles of guest molecules. This expectation realized as a rule for dozens series of inclusion compounds [37, 61, 62], but several investigated cases are different. The studied process of the thermal decomposition of  $[\text{Li}_2\text{Zn}_2(\text{bpdc})_2(\text{dabco})] \cdot 9\text{DMF} \cdot 4\text{H}_2\text{O}$  inclusion compound is the typical exception to the rule.

After the dehydration process, the apparent activation energy of 9 mol DMF single-stage removal ( $70 \text{ kJ mol}^{-1}$  of the inclusion compound) does not correspond to the heat of the nine DMF moles vaporization ( $\Delta H_{\text{vapor}} \approx 380 \text{ kJ}$ ), but corresponds to the vaporization heat of pure liquid DMF compound ( $\Delta H_{\text{vapor}} = 42.3 \text{ kJ mol}^{-1}$  of DMF). It can be explained by the full framework destruction during the water removal with the formation of the solid–liquid mixture. In this case, the DMF removal is the vaporization of the DMF drop (dispersed in the amorphous powder), and the apparent activation energy of the process is  $E = 70 \text{ kJ mol}^{-1}$  of DMF (not per mole of inclusion

compound). Therefore, this apparent activation energy fits to the heat of DMF vaporization.

If the thermal decomposition of the inclusion compounds on the basis of microporous metal–organic frameworks is attended by the guest-free structure collapse, the solid–liquid mixture (the simple coordination compounds + guest and linkers) is formed. The kinetics of the multistage decomposition will involve the vaporization stages of the free volatile guest compounds from this mixture. The values of the apparent activation energy refer not to the decomposition of the inclusion compound mole, but refer to the evaporating process of the guest (or linker) mole.

**Acknowledgements** The authors thank the Russian Foundation for Basic Research for the financial support (Grant No. 17–53–16015).

## References

- Karami K, Naeini NH, Eigner V, Dusek M, Lipkowski J, Herves P, Tavako H. Palladium complexes with 3-phenylpropylamine ligands: synthesis, structures, theoretical studies and application in the aerobic oxidation of alcohols as heterogeneous catalysts. *RSC Adv.* 2015;5:102424–35. <https://doi.org/10.1039/c5ra17249g>.
- Karami K, Hashemi S, Lipkowski J, Mardani F, Momtazi-borjani AA, Lighvan ZM. Synthesis, characterization and biological activities of two novel orthopalladated complexes: interactions with DNA and bovine serum albumin, antitumour activity and molecular docking studies. *Appl Organomet Chem.* 2017;31:e3740. <https://doi.org/10.1002/aoc.3740>.
- Karami K, Alinaghi M, Amirghofran Z, Lipkowski J, Momtazi-borjani AA. A saccharinate-bridged palladacyclic dimer with a Pd–Pd bond: experimental and molecular docking studies of the interaction with DNA and BSA and in vitro cytotoxicity against human cancer cell lines. *New J Chem.* 2018;42:574–86. <https://doi.org/10.1039/c7nj03138f>.
- Dağlı O, AliKöse D, İçten O, AlpAvc G, Şahin O. The mixed ligand complexes of Co(II), Ni(II), Cu(II) and Zn(II) with coumarilic acid/1,10-phenanthroline. *J Therm Anal Calorim.* 2018. <https://doi.org/10.1007/s10973-018-7773-y>.
- Vlaicu ID, Olar R, Scăteanu GV, Silvestro L, Maurer M, Stănică N, Badea M. Thermal, spectral and biological investigation of new nickel complexes with imidazole derivatives. *J Therm Anal Calorim.* 2018;134:503–12. <https://doi.org/10.1007/s10973-018-7133-y>.
- Świdzki G, Wilczewska AZ, Świsłocka R, Kalinowska M, Lewandowski W. Spectroscopic (IR, Raman, UV–Vis) study and thermal analysis of 3d-metal complexes with 4-imidazolecarboxylic acid. *J Therm Anal Calorim.* 2018;134:513–25. <https://doi.org/10.1007/s10973-018-7524-0>.
- Magyari J, Holló BB, Rodić MV, Szilágyi IM, Szécsényi KM. Synthesis and characterization of diazine-ring containing hydrazones and their Zn(II) complexes. *J Therm Anal Calorim.* 2018;133:443–52. <https://doi.org/10.1007/s10973-017-6908-x>.
- Jaćimović Z, Kosović M, Kastratović V, Holló BB, Szécsényi KM, Szilágyi IM, Latinović N, Vojinović-Ješić LV, Rodić M. Synthesis and characterization of copper, nickel, cobalt, zinc complexes with 4-nitro-3-pyrazolecarboxylic acid ligand. *J Therm Anal Calorim.* 2018. <https://doi.org/10.1007/s10973-018-7229-4>.

9. Xavier TT, deGois EP, Sarto LE, deAlmeida ET. Thermal behavior study of palladium(II) complexes containing the iminic ligand *N, N'*-bis(3,4-dimethoxybenzaldehyde) ethane-1,2-diamine. *J Therm Anal Calorim.* 2018;134:1829–37. <https://doi.org/10.1007/s10973-018-7429-y>.
10. Diamantis SA, Margariti A, Pournara AD, Papaefstathiou GS, Manos MJ, Lazarides T. Luminescent metal–organic frameworks as chemical sensors: common pitfalls and proposed best practices. *Inorg Chem Front.* 2018;5:1493–511. <https://doi.org/10.1039/C8QI00090E>.
11. Peller M, Böll K, Zimpel A, Wuttke S. Metal-organic framework nanoparticles for magnetic resonance imaging. *Inorg Chem Front.* 2018;5:1760–79. <https://doi.org/10.1039/C8QI00149A>.
12. Gheorghe A, Tepaske MA, Tanase S. Homochiral metal–organic frameworks as heterogeneous catalysis. *Inorg Chem Front.* 2018;5:1512–23. <https://doi.org/10.1039/C8QI00063H>.
13. Mayo RA, Sullivan DJ, Fillion TAP, Kycia SW, Soldatov DV, Preuss KE. Reversible crystal-to-crystal chiral resolution: making/breaking non-bonding S...O interactions. *Chem Commun.* 2017;53:3964–6. <https://doi.org/10.1039/C7CC00907K>.
14. Okeke EB, Soldatov DV. Coordination and inclusion compounds formed by addition of quinoline (Q) or isoquinoline (Iq) to a metal(II) dibenzoylmethanate (Co, Ni, Zn, Cd). Composition, structure and thermal dissociation properties. *J Therm Anal Calorim.* 2010;100:801–10. <https://doi.org/10.1007/s10973-010-0689-9>.
15. Kleist W, Maciejewski M, Baiker A. MOF-5 based mixed-linker metal–organic frameworks: synthesis, thermal stability and catalytic application. *Thermochim Acta.* 2010;499:71–8. <https://doi.org/10.1016/j.tca.2009.11.004>.
16. Lee CH, Soldatov DV, Tzeng CH, Lai LL, Lu KL. Design of a peripheral building block for H-bonded dendritic frameworks and analysis of the void space in the bulk dendrimers. *Sci Rep.* 2017. <https://doi.org/10.1038/s41598-017-03684-y>.
17. Guillerm V, Kim D, Eubank JF, Luebke R, Liu X, Adil K, Lah MS, Eddaoudi M. A supermolecular building approach for the design and construction of metal–organic frameworks. *Chem Soc Rev.* 2014;43:6141–72. <https://doi.org/10.1039/C4CS00135>.
18. Farha OK, Hupp JT. Rational design, synthesis, purification, and activation of metal–organic framework materials. *Acc Chem Res.* 2010;43:1166–75. <https://doi.org/10.1021/ar1000617>.
19. Zhang Z, Zhao Y, Gong O, Li Z, Li J. MOFs for CO<sub>2</sub> capture and separation from flue gas mixtures: the effect of multifunctional sites on their adsorption capacity and selectivity. *Chem Commun.* 2013;49:653–61. <https://doi.org/10.1039/C2CC35561B>.
20. Bae Y-S, Snurr RQ. Development and evaluation of porous materials for carbon dioxide separation and capture. *Angew Chem Int Ed.* 2011;50:11586–96. <https://doi.org/10.1002/anie.201101891>.
21. Tranchemontagne DJ, Park KS, Furukawa H, Eckert J, Knobler CB, Yaghi OM. Hydrogen storage in new metal–organic frameworks. *J Phys Chem C.* 2012;116:13143–51. <https://doi.org/10.1021/jp302356q>.
22. Langmi HW, Ren J, North B, Mathe M, Bessarabov D. Hydrogen storage in metal–organic frameworks: a review. *Electrochim Acta.* 2014;128:368–92. <https://doi.org/10.1016/j.electacta.2013.10.190>.
23. Yu Y, Ren Y, Shen W, Deng H, Gao Z. Applications of metal–organic frameworks as stationary phases in chromatography. *TrAC (Trends Anal Chem).* 2013;50:33–41. <https://doi.org/10.1016/j.trac.2013.04.014>.
24. Van de Voorde B, Bueken B, Denayer J, De Vos D. Adsorptive separation on metal–organic frameworks in the liquid phase. *Chem Soc Rev.* 2014;43:5766–88. <https://doi.org/10.1039/C4CS00006D>.
25. Liu J, Chen L, Cui H, Zhang J, Zhang L, Su C-Y. Applications of metal–organic frameworks in heterogeneous supramolecular catalysis. *Chem Soc Rev.* 2014;43:6011–61. <https://doi.org/10.1039/C4CS00094C>.
26. Liu Y, Xuan W, Cui Y. Engineering homochiral metal-organic frameworks for heterogeneous asymmetric catalysis and enantioselective separation. *Adv Mater.* 2010;22:4112–35. <https://doi.org/10.1002/adma.201000197>.
27. Hu Z, Deibert BJ, Li J. Luminescent metal–organic frameworks for chemical sensing and explosive detection. *Chem Soc Rev.* 2014;43:5815–40. <https://doi.org/10.1039/C4CS00010B>.
28. Pramanik S, Hu Z, Zhang X, Zheng C, Kelly S, Li J. A systematic study of fluorescence-based detection of nitroexplosives and other aromatics in the vapor phase by microporous metal-organic frameworks chemistry. *Eur J.* 2013;19:15964–71. <https://doi.org/10.1002/chem.201301194>.
29. Desai AW, Manna B, Karmakar A, Sahu A, Ghosh SK. A water-stable cationic metal–organic framework as a dual adsorbent of oxoanion pollutants. *Angew Chem Int Ed.* 2016;55:7811–5. <https://doi.org/10.1002/anie.201600185>.
30. Cunha D, Yahia MB, Hall S, Miller SR, Chevreau H, Elkaïm E, Maurin G, Horcajada P, Serre C. Rationale of drug encapsulation and release from biocompatible porous metal-organic frameworks. *Chem Mater.* 2013;25:2767–76. <https://doi.org/10.1021/cm400798p>.
31. Sun C-Y, Qin C, Wang C-G, Su Z-M, Wang S, Wang X-L, Yang G-S, Shao K-Z, Lan Y-Q, Wang E-B. Chiral nanoporous metal–organic frameworks with high porosity as materials for drug delivery. *Adv Mater.* 2011;23:5629–32. <https://doi.org/10.1002/adma.201102538>.
32. Goesten MG, Juan-Alcañiz J, Ramos-Fernandez EV, Gupta KBSS, Stavitski E, van Bekkum H, Gascon J, Kapteijn F. Sulfation of metal–organic frameworks: opportunities for acid catalysis and proton conductivity. *J Catal.* 2011;281:177–87. <https://doi.org/10.1016/j.jcat.2011.04.015>.
33. Serre C, Mellot-Draznieks C, Surlé S, Audebrand N, Filinchuk Y, Férey G. Role of solvent-host interactions that lead to very large swelling of hybrid frameworks. *Science.* 2007;315:1828–31. <https://doi.org/10.1126/science.1137975>.
34. Han J, Wang D, Du YH, Xi S, Chen Z, Yin S, Zhou T, Xu R. Polyoxometalate immobilized in MIL-101(Cr) as an efficient catalyst for water oxidation. *Appl Catal A.* 2016;521:83–9. <https://doi.org/10.1016/j.apcata.2015.10.015>.
35. Dyadin YA, Soldatov DV, Logvinenko VA, Lipkovsky J. Contact stabilization of host complex molecules during clathrate formation: the pyridine-zinc nitrate and the pyridine-cadmium nitrate systems. *J Coord Chem.* 1996;37:63–75.
36. Sapijanik AA, Kiskin MA, Samsonenko DG, Ryadun AA, Dybtsev DN, Fedin VP. Luminescence sensing by coordination polymers derived from a pre-organized heterometallic carboxylic building unit. *Polyhedron.* 2018;145:147–53. <https://doi.org/10.1016/j.poly.2018.02.007>.
37. Logvinenko V, Dybtsev D, Fedin V, Drebuschak V, Yutkin M. The stability of inclusion compounds under heating. Part 2. Inclusion compounds of layered zinc camphorate, linked by linear N-donor ligands. *J Therm Anal Calorim.* 2010;100:183–9.
38. Netzsch Thermokinetics. <http://www.netzsch-thermal-analysis.com/us/products-%20%20solutions/advanced-software/thermo-kinetics.html>.
39. Moukhina E. Determination of kinetic mechanisms for reactions measured with thermoanalytical instruments. *J Therm Anal Calorim.* 2012;109:1203–14.
40. Kissinger HE. Reaction kinetics in differential thermal analysis. *Anal Chem.* 1957;29:1702–6.
41. Friedman HL. Kinetics of thermal degradation of char-forming plastics from thermogravimetry. *J Polym Sci.* 1963;6:183–95.



42. Ozawa T. A new method of analyzing thermogravimetric data. *Bull Chem Soc Japan*. 1965;38:1881–6.
43. Ozawa T. Estimation of activation energy by isoconversion methods. *Thermochim Acta*. 1992;203:159–65.
44. Flynn JH, Wall LA. General treatment of the thermogravimetry of polymers. *J Res Nat Bur Stand*. 1966;70:478–523.
45. Opfermann J, Kaisersberger E. An advantageous variant of the Ozawa–Flynn–Wall analysis. *Thermochim Acta*. 1992;203:167–75.
46. Opfermann JR, Kaisersberger E, Flammersheim HJ. Model-free analysis of thermo-analytical data—advantages and limitations. *Thermochim Acta*. 2002;391:119–27.
47. Vyazovkin S. Model-free kinetics: staying free of multiplying entities without necessity. *J Therm Anal Calorim*. 2006;83:45–51.
48. Simon P. Single-step kinetics approximation employing nonarrhenius temperature functions. *J Therm Anal Calorim*. 2005;79:703–8.
49. Simon P. The single-step approximation: attributes, strong and weak sides. *J Therm Anal Calorim*. 2007;88:709–15.
50. Borchard HJ, Daniels F. The application of differential thermal analysis to the study of reaction kinetics. *J Am Chem Soc*. 1957;79:41–6.
51. Vyazovkin S, Burnham AK, Criado JM, Luis A, Perez-Maqueda LA, Popescu C, Sbirrazzuoli N. ICTAC Kinetics Committee recommendations for performing kinetic computations on thermal analysis data. *Thermochim Acta*. 2011;520:1–19.
52. Vyazovkin S, Chrissafis K, Di Lorenzo M-R, Koga N, Pijolat M, Roduit B, Sbirrazzuoli N, Suñol J-J. ICTAC Kinetics Committee recommendations for collecting experimental thermal analysis data for kinetic computations. *Thermochim Acta*. 2014;590:1–23.
53. Vyazovkin S. *Isoconversional kinetics of thermally stimulated processes*. Berlin: Springer; 2015.
54. Simon P, Thomas P, Dubaj T, Cibulkova Z, Peller A, Veverka M. The mathematical incorrectness of the integral isoconversional methods in case of variable activation energy and the consequences. *J Therm Anal Calorim*. 2014;115:853–9.
55. Simon P, Dubaj T, Cibulkova Z. Equivalence of the Arrhenius and non-Arrhenian temperature functions in the temperature range of measurement. *J Therm Anal Calorim*. 2015;120:231–8.
56. Sestak J. Is the original Kissinger equation obsolete today: not obsolete the entire non-isothermal kinetics? *J Therm Anal Calorim*. 2014;117:3–7.
57. Galwey AK. What theoretical and/or chemical significance is to be attached to the magnitude of an activation energy determined for a solid-state decomposition by thermal analysis? *J Therm Anal Calorim*. 2006;86:267–86.
58. Roura P, Farjas J. Analytical solution for the Kissinger equation. *J Mater Res*. 2009;24:3095–8.
59. Holba P, Šesták J. Imperfections of Kissinger evaluation method and crystallization kinetics (translation from Russian journal). *Glass Phys Chem*. 2014;40:486–91.
60. Dubaj T, Cibulková Z, Šimon P. An incremental isoconversional method for kinetic analysis based on the orthogonal distance regression. *J Comput Chem*. 2015;36:392–8.
61. Logvinenko V. Stability and reactivity of coordination and inclusion compounds in the reversible processes of thermal dissociation. *Thermochim Acta*. 1999;340–341:293–9.
62. Logvinenko V, Drebuschak V, Pinakov D, Chekhova G. Thermodynamic and kinetic stability of inclusion compounds under heating. *J Therm Anal*. 2007;90:23–30.
63. Lomovsky O, Bychkov A, Lomovsky I, Logvinenko V, Burdukov A. Mechanochemical production of lignin-containing powder fuels from biotechnical industry waste: a review. *Therm Sci*. 2015;19:219–29.
64. Vasilyeva I, Logvinenko V. Contribution of chemical methods to the study of nanostructure of ultrafine and amorphous materials. *Solid State Phenom*. 2017;257:237–40.
65. Logvinenko VA, Makotchenko VG, Fedorov VE. Reactivity in combustion process for expanded graphites: influence of dimensional effect. *Nanosyst Phys Chem Math*. 2016;7:234–43.
66. Makotchenko VG, Pinakov DV, Logvinenko VA. The influence of dimensional effects on the composition and properties of polycarbonfluoride. *Chem Asian J*. 2015;10:1761–7.
67. Chekhova GN, Pinakov DV, Shubin YuV, Logvinenko VA. Structural rearrangements of the inclusion compound of fluorinated graphite with acetonitrile during isothermal deintercalation. *J Therm Anal Calorim*. 2017;128:349–55. <https://doi.org/10.1007/s10973-016-5846-3>.
68. Bushuev MB, Pishchur DP, Logvinenko VA, Gatilov YuV, Korolkov IV, Shundrina IK, Nikolaenkova EB, Krivopalov VP. Mononuclear iron(II) complex: cooperativity, kinetics and activation energy of the solvent-dependent spin transition. *Dalton Trans*. 2016;45:107–20.
69. Krisyuk VV, Baidina IA, Kryuchkova NA, Logvinenko VA, Plyusnin PE, Korolkov IV, Zharkova GI, Turgambaeva AE, Igumenov IK. Volatile heterometallics: structural diversity of palladium-lead  $\beta$ -diketonates and correlation with thermal properties. *Dalton Trans*. 2017;46:12245–56. <https://doi.org/10.1039/c7dt02843a>.

**Publisher's Note** Springer Nature remains neutral with regard to jurisdictional claims in published maps and institutional affiliations.